

Drag reduction of a disk with an upstream rod

Panfeng Zhang[†], Lei Gao[‡], and Jinjun Wang^{††}

Institute of Fluid Mechanics, Beijing University of Aeronautics & Astronautics, Beijing, 10083, P. R. China

(Received November 3, 2005, Accepted April 21, 2006)

Abstract. The pressure and drag measurements were carried out in the wind tunnel to investigate the drag reduction of the disk by using an interference rod placed upstream. The results indicate that there is a pair of standing vortices in the front stagnation region of the disk induced by the rod. The standing vortices can decrease the pressure on the disk upwind side; hence it can reduce the drag of the disk. With an increasing rod diameter, the standing vortices are strengthened and more drag reduction can be achieved for the disk. With rod diameter $d/D = 0.05$ (d, D are the diameters of rod and disk, respectively), the total drag of the disk can be reduced by about 9% compared with that of the bare disk.

Keywords: drag reduction; disk; interference rod; pressure measurement.

1. Introduction

The flow around bluff bodies is a classical subject in fluid mechanics, and the drag of this kind of body endures more drag than the streamlined body such as airfoil when they are immersed in the moving fluid. In many engineering applications, it is required that the drag of bluff bodies should be reduced for different purposes. A lot of passive flow control methods were proposed to reduce the bluff body drag. For example, use of surface processes like roughness and riblet films, use of a splitter plate or rod downstream of cylindrical body and use of slits along the cylinder's axis are well known.

Based on the understanding of the flow around two equal cylinders in tandem, Lesage and Gartshore (1987) proposed a method to reduce the cylinder drag by using an upstream rod. When the spacing between the rod and the cylinder is small enough, there exists a cavity flow region with low pressure between them, which results in more drag reduction of the cylinder. They utilized a rod with diameter $d/D = 0.25$, where d and D are diameters of the rod and the cylinder, respectively, the circular cylinder drag could be reduced by 73%. Igarashi (1997), Prasad and Williamson (1997) also reduced the drag of circular/square cylinder by an upstream interference like using a small rod or flat plate. Zhang, *et al.* (2005, 2006) investigated this passive drag reduction method by hydrogen bubble techniques and pressure measurement. They also found that the drag of the bluff body (circular cylinder or prism cylinder) could be reduced by an upstream rod in the cavity flow mode.

[†] Post Doctor, E-mail: pfzhang@ase.buaa.edu.cn

[‡] Graduate Studnet, E-mail: tarzan@ase.buaa.edu.cn

^{††} Professor, Corresponding Author, E-mail: jjwang@buaa.edu.cn

In flow visualization, they indicated there exist a pair of standing vortices between the interference rod and the bluff body, which results in the low pressure on the upwind side of the bluff body. For 3D bluff bodies, Wang, *et al.* (2006) and Lian and Su (1993) also exhibited standing vortices in the front stagnation region of the disk in water tunnel. It is, therefore, considered that the upstream rod might reduce the drag of 3D bluff bodies through the formation of the standing vortices. The present work is to investigate the pressure distribution and drag characteristics of the disk induced by an upstream rod in wind tunnel, and the effects of the rod diameter and location on the aerodynamic characteristics of the disk were presented.

2. Experiments setup and equipments

The experiments were conducted in D4 open-circuit wind tunnel of Beijing University of Aeronautics & Astronautics. The test section of the tunnel is $1.5\text{ m} \times 1.5\text{ m}$, where the turbulence level was less than 0.1%. The disk that was made of plexiglass with diameter $D=200\text{ mm}$ was mounted to the strain balance from rear side and normal to the incoming flow. This configuration yielded blockage ratio of 4%. Rods with diameter $d/D=0.005, 0.01, 0.03$ and 0.05 were set at the horizontal symmetry plane of the disk and also normal to the flow. The distance L between the centers of the rod and the disk varied from $0.1D$ to $4D$. The setup configuration is sketched in Fig. 1. The free stream velocity was $U_0=20\text{ m/s}$, which yields the Reynolds number based on the disk diameter was $Re=2.74 \times 10^5$ and the Reynolds numbers based on the rod diameter were from 1.37×10^3 to 1.37×10^4 .

There are two models used in this experiment. One is a bare disk used in drag force measurements, the other is a disk with 122 pressure ports on the upwind side used in pressure measurement. This consideration is necessary to avoid the pressure tube interference to the drag force measurement. The drag data is obtained with an internal, six-component, strain gauge balance. The pressure is measured by the PSI NetScanner 9816 rackmount intelligent pressure scanner. The sample frequency is 20 Hz and the total period of the sampling is 10 seconds. The drag coefficient and the pressure coefficient were normalized by the dynamic pressure measured by the pitot tube. The uncertainties of the pressure and drag coefficient are 3% and 1%, respectively.

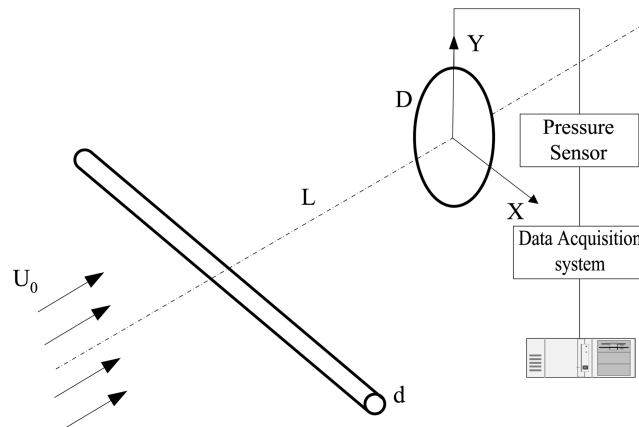


Fig. 1 The sketch of the experiment setup

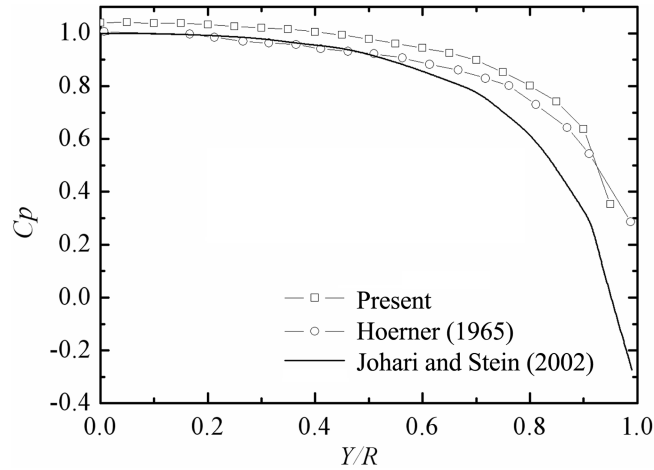


Fig. 2 The pressure distribution on the radial direction of the disk

Fig. 2 shows the pressure distribution along the radial direction of the disk upwind side (R is the radius of the disk), where the previous results Hoerner (1965), Johari and Stein (2002) are also included for comparison. The present curve is similar to reference Hoerner (1965), where a constant offset was introduced by the uncertainty of the dynamic pressure measured by the pitot tube. The pressure coefficient in reference Johari and Stein (2002) is much lower near the disk edge, which is obtained on the impulsively started disk by numerical simulation. The drag coefficient of the bare disk measured by the strain balance is 1.21, this value is very close to 1.14 and 1.17 obtained by Hoerner (1965) and Johari and Stein (2002). So the present methods for pressure and drag measurements are reasonable for investigating the aerodynamics of the disk.

3. Experimental results and discussions

3.1. Pressure distribution on the disk

Fig. 3 presents the contours of pressure on the bare disk upwind side, which serves as a

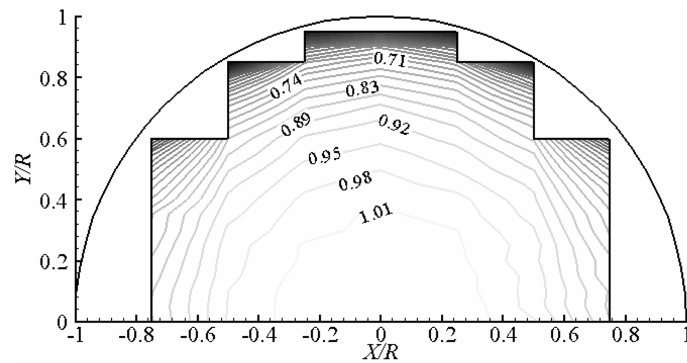


Fig. 3 The contours of pressure on the bare disk upwind side

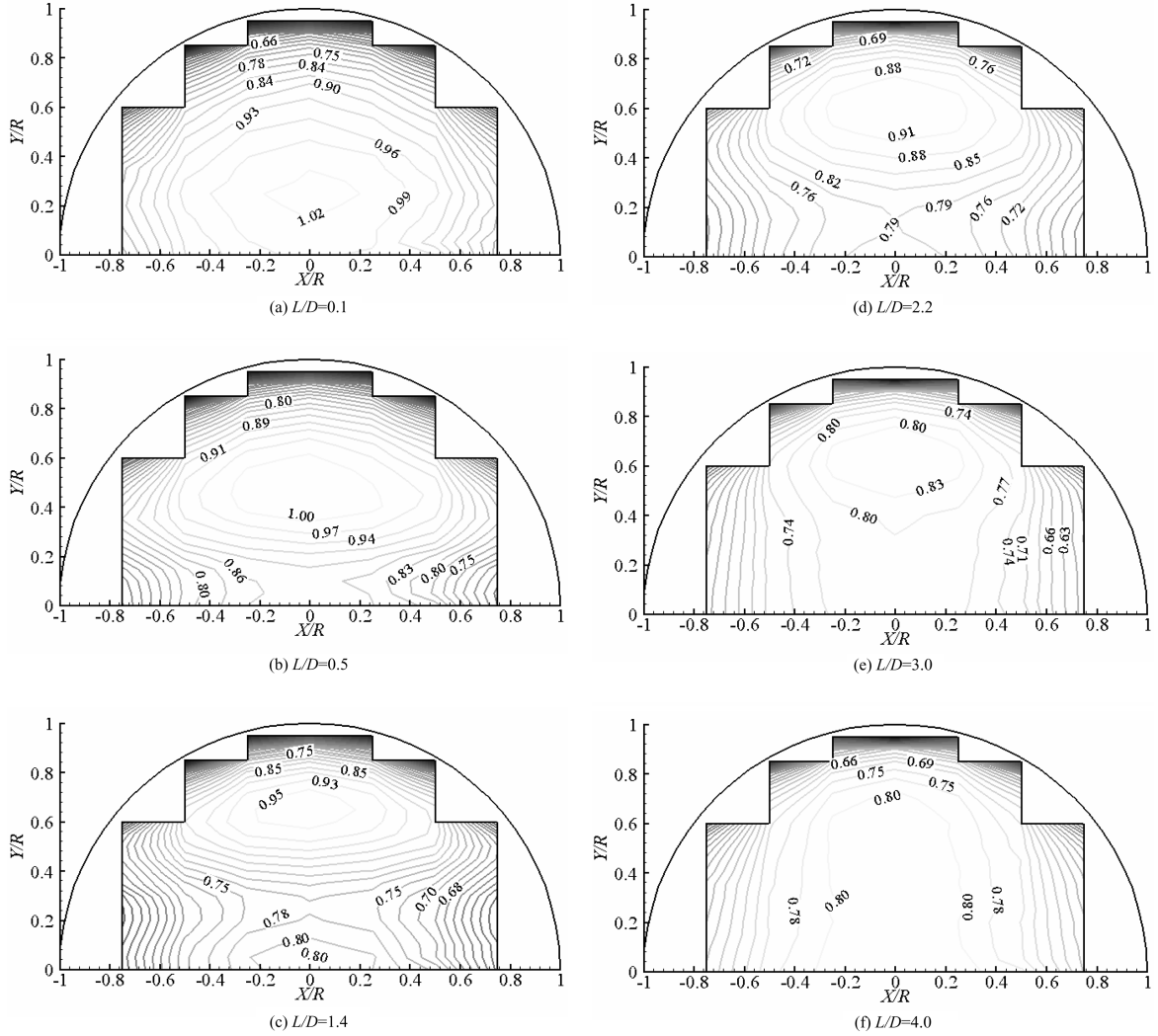


Fig. 4 The pressure distribution vs. spacing L/D

baseline for comparison. The pressure is constant at 1.0 around the stagnation point of the disk at $r/R < 0.4$ (here r is the radial distance from the center of the disk). With an increasing r , the pressure drops rapidly because of the flow acceleration over the disk. The pressure distribution is nearly axisymmetric, indicating that the model is perpendicular to the incoming flow. The contours in Fig. 4 present the variation of pressure distribution for the non-dimensional distance $L/D = 0.1 \sim 4.0$ and $d/D = 0.05$. With an upstream rod at $L/D = 0.1$ (Fig. 4a), there is a low-pressure region near the horizontal symmetric axis of the disk ($Y=0$), which is induced by the velocity deficit in the rod wake. The maximum pressure appears at $X/R = 0$, $Y/R = 0.22$, associated with the attachment of rod's separated shear layer. For a 2D interference rod, the separated shear layer should attach to a line ($Y/R = \text{constant}$) on the disk. Due to the 3D flow structure around the disk, the flow begins to accelerate near the disk edge, which results in the

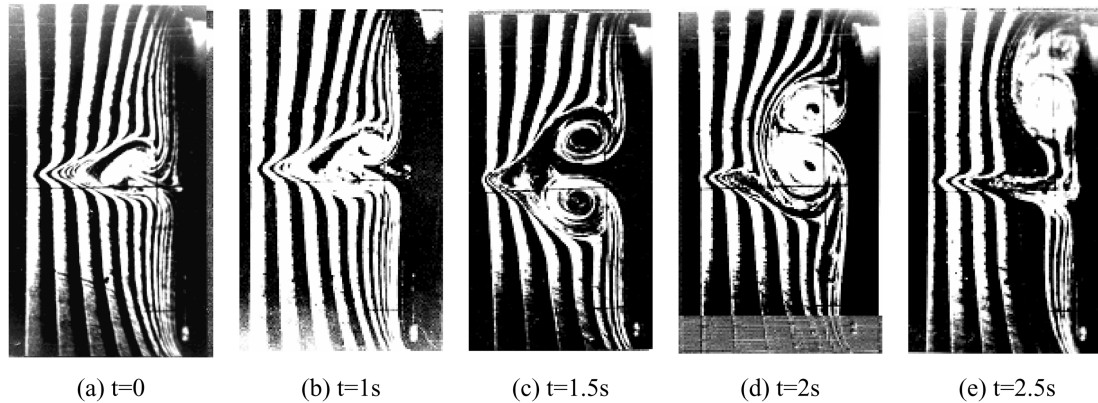


Fig. 5 The evolution of the standing vortices in the front stagnation region of the disk induced by the upstream interference wire (Wang, *et al.* 2005)

maximum pressure point at $X/R = 0$, $Y/R = 0.22$. With the increasing the distance ($L/D = 0.5$), the rod wake becomes wider, and the maximum pressure point moves to $Y/R = 0.5$. Whilst the minimum pressure appears at $Y/R = 0.15$, and the origin again has the local maximum pressure. When the distance L/D increases to 1.4, it is more obvious that the local maximum pressure appears at the origin, which can be seen by circles around the origin in the contour map. This pressure distribution can be explained from the flow structures. Wang, *et al.* (2005) observed a pair of standing vortices near the front stagnation region of the disk induced by a fine interference wire as shown in Fig. 5 (the wire diameter in the experiments is 0.1~0.3 mm, the Reynolds number based on the disk diameter is 7.0×10^3). Lian and Su (1993) concluded that no matter the vortex sheds from the wire or not, the wire can induce a pair of standing vortices in the front stagnation region of the bluff bodies with a large flat upwind side. Although the rod diameter in present study is much larger than the wire diameter in reference Wang, *et al.* (2005), the flow structure should be similar. Zdravkovich (1997), Slaoutiand and Stansby (1992) also presented a similar pair of standing vortices between two circular cylinders in tandem in cross flow. So the two points with the maximum pressure are corresponding to the attachment of the rod separated shear layer and the separated saddle point on the disk, respectively. The curve with low pressure is corresponding to the center of the standing vortices. For small L/D , the standing vortices have small length scale and the spatial resolution of the pressure ports can not exhibit the pressure variation induced by the standing vortices, except that the standing vortices are strong enough at $L/D = 1.4$. At a great distance ($L/D = 3.0$), the vortices are shed from the rod onto a disk, which is similar to the wake impinging mode in 2D flow (Igarashi 1997, Prasad and Williamson 1997, Zhang, *et al.* 2005). The curve with low pressure disappears and only the point with maximum pressure exists on the disk. With $L/D = 4.0$, the rod wake is wider than the disk, the pressure distribution over the disk becomes similar to that on the bare disk in cross flow.

3.2. Pressure distribution along the vertical symmetric axis

Fig. 6 shows the pressure distribution along the vertical symmetric axis on the disk vs. the non-dimensional distance L/D for $d/D = 0.05$. The pressure distribution is similar to that shown in Fig. 4,

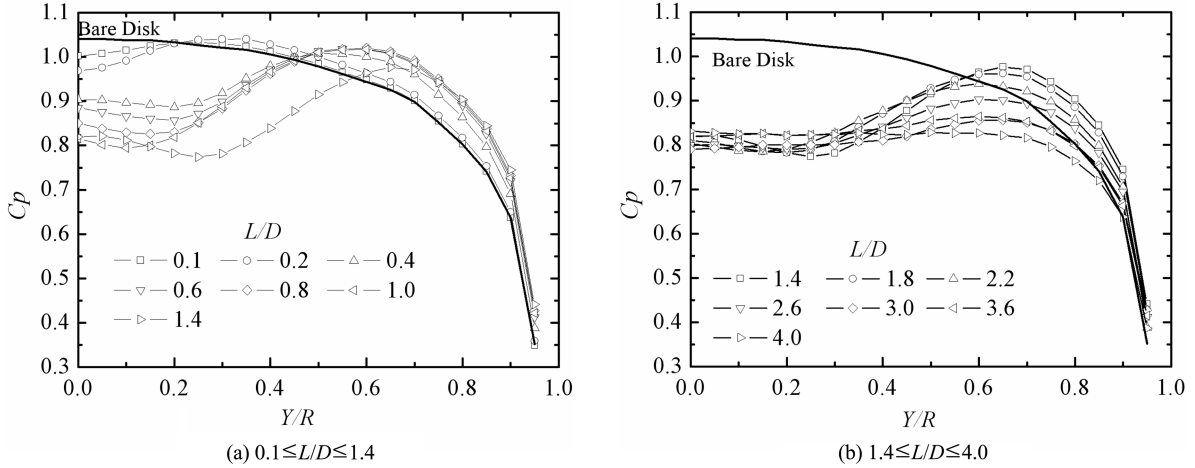


Fig. 6 Pressure distribution at the symmetric line(Y axis) of the disk vs. the non-dimensional distance L/D ($d/D = 0.05$)

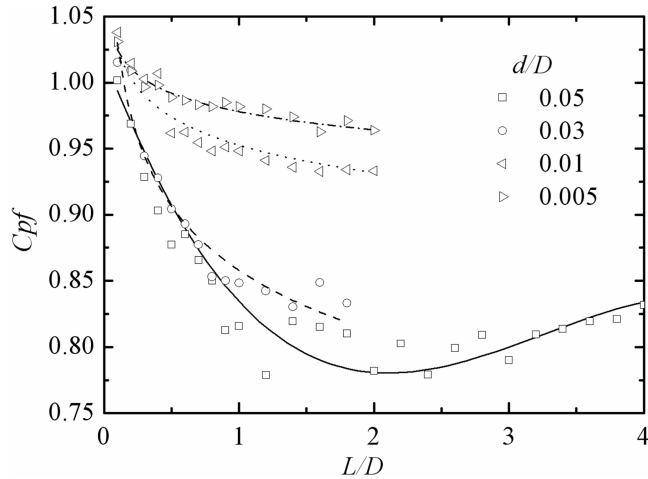


Fig. 7 The pressure at the centre point of the disk C_{pf} vs. L/D

and the curve at $L/D = 1.4$ is a typical pressure distribution of the standing vortices. The pressure distribution along the vertical symmetric axis on the disk with different rod diameters can also exhibit similar variations of the standing vortices formation, evolution and disappearance (not presented here). Fig. 7 presents the variation of the stagnation pressure on the disk center C_{pf} with different rod diameter d/D and the non-dimensional distance L/D , where curves are fitted through experimental data points. For $d/D = 0.05$, C_{pf} decreases rapidly with an increasing L/D , corresponding to the strength decrease of the standing vortices. After C_{pf} reaches its minimum value, it increases again with L/D , due to the standing vortices vanishing at large L/D and the velocity deficit of rod wake begins to recover with L/D increase. The trend of the curves are similar to each others at the section $L/D \leq 2.0$, but C_{pf} has lower value as the rod diameter increases. This

indicates that there is more drag reduction with larger rod diameter.

3.3. Drag reduction of the disk

The fore-body drag coefficient of the disk $C_{D(\text{forebody})}$ can be obtained by integrating the pressure distribution on its upwind side:

$$C_{D(\text{forebody})} = \frac{\sum_{i=1}^n C p_i S_i}{\sum_{i=1}^n S_i}$$

here $C p_i$ is the pressure at different elements, S_i is the element area, and n is the total number of the elements. Fig. 8 shows $C_{D(\text{forebody})}$ vs. L/D with different d/D . For $d/D=0.05$, the fore-body drag of the disk decreases with an increasing L/D . This trend is different with that of C_{pf} , which has its minimum value at $L/D=2.0$. This difference can be explained as follows: for $L/D > 2.0$, the C_{pf} increases with L/D , but the pressure near the edge of the disk ($Y/R=0.7$) goes to decrease as shown in Fig. 6(b). The combined effects result in the fore-body drag decreases with L/D increase. At $L/D=4.0$, the fore-body drag of the disk can be reduced by about 17% that of the bare disk. For rod diameters $d/D=0.005\sim 0.03$, the fore-body drag of the disk vs. L/D falls in nearly the same curve, and the maximum fore-body drag reduction is about 3%.

Fig. 9 presents the relative drag coefficient of a disk obtained by the strain gauge balance vs. L/D , where C_{D0} is the drag coefficient of the bare disk. For fine rods ($d/D=0.005, 0.01$), the disk drag does not change with L/D . For rod diameters $d/D=0.03, 0.05$, there seems to exist an optimum distance L/D , at which the rod has maximum efficiency in reducing the disk drag. For $d/D=0.05$,

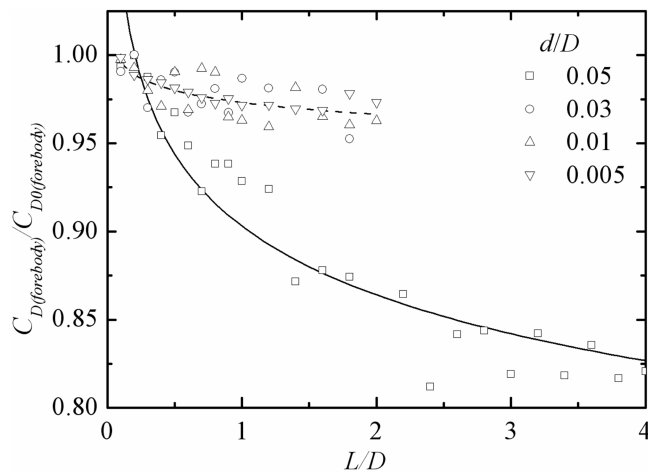


Fig. 8 The relative fore-body drag coefficient of the disk vs. L/D

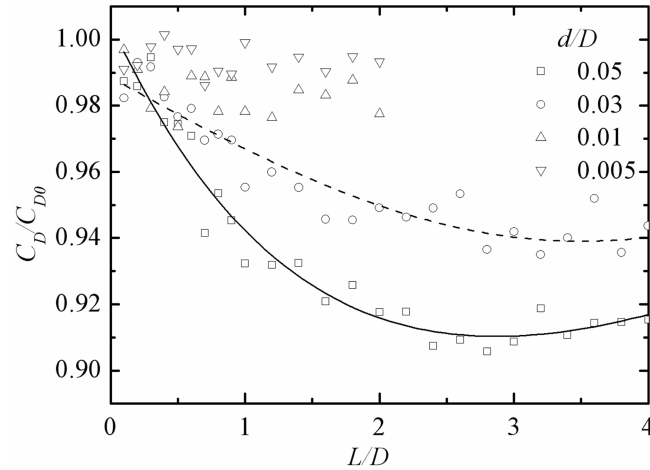


Fig. 9 The relative drag coefficient of the disk vs. L/D

the optimum L/D for drag reduction coincides to that with minimum center point pressure C_{pf} as shown in Fig. 7, which indicates that the maximum disk drag reduction occurs at the switch point of two different flow patterns. They are the standing vortices for $L/D < 2.0$ and the wake impinging mode for $L/D > 2.0$ as mentioned in section 3.1. This feature is similar to that in 2D investigations (Igarashi 1997, Prasad and Williamson 1997, Zhang, *et al.* 2005). The total drag reduction of the disk is about 9% with $d/D = 0.05$, which is much less than the fore-body drag reduction by integrating the pressure distribution in Fig. 8. The region adopted in pressure integration causes this difference. If the region near the disk edge were also added in pressure integration, the fore-body drag reduction would not be so much as that shown in Fig. 8. Another probable reason is the variation of the aft-body drag of the disk. From the conclusion about 2D flow (Igarashi 1997, Prasad and Williamson 1997, Zhang, *et al.* 2005), the rear base pressure of the flat plate would not change with an upstream rod, for its shear layer separates at sharp edge. But the flow around the disk is so complicated, which has random shedding hairpin vortex and instability in the shear layer caused by the helix vortex (Cannon, *et al.* 1993, Miao, *et al.* 1997). There are no sufficient literatures about the effects of incoming flow condition on the vortex shedding, drag and rear base pressure of the disk. So the flow characteristics of the 3D disk can not be derived from that of the 2D flat plate, even 3D flow around the sphere (Kiya 2001). The influence of the upstream rod on the rear base suction pressure of the disk is worth further investigating in the future.

4. Conclusions

The main results of the present work can be summarized as follows:

- (1) The pressure distribution of the disk is affected by the non-dimensional distance L/D , corresponding to the formation, evolution and disappearance of the standing vortices in the front stagnation region of the disk.
- (2) The standing vortices induced by the upstream rod can decrease the pressure on the disk upwind side, meanwhile resulting in the drag reduction of the disk. With an increasing rod diameter, the standing vortices are strengthened and more drag reduction of the disk can be

obtained. For $d/D = 0.05$, the total drag reduction of the disk is about 9% that of the bare disk.

Notation

- C_D , drag of the disk obtained by strain balance
 $C_{D(\text{forebody})}$, forebody drag of the disk obtained by pressure integration
 C_{pf} , stagnation pressure coefficient on the disk center
 C_{p_i} , pressure coefficient at different elements
 d , rod diameter
 D , disk diameter
 L , center to center spacing distance between the rod and the disk
 n , total number of the elements
 r , radial coordinate of a point on the disk
 R , disk radius
 Re , Reynolds number
 S_i , element area
 U_0 , freestream velocity
 X , horizontal coordinate of a point on the disk
 Y , vertical coordinate of a point on the disk

Acknowledgements

The present research was supported by the National Natural Science Foundation of China under grant no. NSFC-10272016 and NSFC-10425207.

References

- Cannon, S., Champagne, F., and Glezer, A. (1993), "Observations of large-scale structures in wakes behind axisymmetric bodies", *Experiments in Fluids*, **14**, 447-450.
 Hoerner, S. F. (1965), "Fluid-dynamic drag", published by the author, Midland Park, NJ.
 Igarashi, T. (1997), "Drag reduction of a square prism by flow control using a small rod", *J. Wind Eng. Ind. Aerodyn.*, **69-71**, 141-153.
 Johari, H. and Stein, K. (2002), "Near wake of an impulsively started wake", *Physics of Fluids*, **14**(10) 3459-3474.
 Kiya, M., Ishikawa, H., and Sakamoto, H. (2001), "Near-wake instabilities and vortex structures of three-dimensional bluff bodies: A review", *J. Wind Eng. Ind. Aerodyn.*, **89**, 1219-1232.
 Lesage, F. and Gartshore, I. S. (1987), "A method of reducing drag and fluctuating side force on bluff bodies", *J. Wind Eng. Ind. Aerodyn.*, **25**, 229-245.
 Lian, Q. X. and Su, Z. Z. (1993), "The standing vortex in the front stagnation region of square plate induced by the fine interference wire", *Science in China*(Series A), **23**(17), 1171-1177.
 Miao, J. J., Leu, T. S., Kiu, T. W., and Chou, J. H. (1997), "On vortex shedding behind a circular disk", *Experiments in Fluids*, **23**, 225-233.
 Prasad, A. and Williamson, C. H. K. (1997), "A method for the reduction of bluff body drag", *J. Wind Eng. Ind. Aerodyn.*, **69-71**, 155-167.
 Slaoutiand, A. and Stansby, P. K. (1992), "Flow around two circular cylinders by the random-vortex method", *J. Fluids Struct.*, **6**, 641-670.
 Wang, J. J., Guo, H., Lian, Q. X., and Choi, K. S. (2005), "The generation of large counter-rotating vortex pair by a very weak shear layer", submitted to *Physics of Fluids*.

- Wang, J. J., Zhang, P. F., Lu, S. F., and Wu, K. (2006), "Drag reduction of a circular cylinder using an upstream rod", *Flow, Turbulence and Combustion*, **76**(1), 83-101.
- Zdravkovich, M. M. (1977), "Review of flow interference between two circular cylinders in various arrangements", *J. Fluids Eng.*, **199**, 618-633.
- Zhang, P. F., Wang, J. J., Lu, S. F., and Mi, J. (2005), "Aerodynamic characteristics of a square cylinder with a rod in staggered arrangement", *Experiments in Fluids*, **38**(4), 494-502.